Research Article Vol. 58, No. 20 / 10 July 2019 / Applied Optics 5479

applied optics

Tunable triangular frequency modulated microwave waveform generation with improved linearity using an optically injected semiconductor laser

Bowen Zhang,[1] Dan Zhu,[1,2] Pei Zhou,[1] Chenxu Xie,[1] and Shilong Pan[1,3]

[1]Key Laboratory of Radar Imaging and Microwave Photonics, Ministry of Education, Nanjing University of Aeronautics and Astronautics, Nanjing 210016, China
[2]e-mail: danzhu@nuaa.edu.cn
[3]e-mail: pans@nuaa.edu.cn

Received 23 April 2019; revised 14 June 2019; accepted 17 June 2019; posted 17 June 2019 (Doc. ID 365790); published 9 July 2019

A photonic approach to generating a triangular frequency modulated microwave waveform with improved linearity using an optically injected semiconductor laser is proposed and demonstrated. By controlling the optical injection strength to the semiconductor laser at the period-one oscillation state to have a triangular shape, a triangular frequency modulated microwave waveform is generated after the optical-electrical conversion. A method based on a generalized regression neural network is proposed to improve the linearity of the generated waveform. By adjusting the parameters of the low-frequency electrical triangular control signal, the tunability of the center frequency, bandwidth, and time duration of the generated waveform can be realized. In the proof-of-concept experiment, a triangular frequency modulated microwave waveform with a frequency range from 14–24 GHz and a time duration of 2 μs has been successfully generated. The improvement of the linearity of the waveform is experimentally verified. The performance of the generated triangular frequency modulated microwave waveforms for reducing the range–Doppler coupling is verified through the analyses of the ambiguity function. The tunability of the center frequency, bandwidth, and time duration is also experimentally demonstrated.

https://doi.org/10.1364/AO.58.005479

1. INTRODUCTION

Thanks to the capability of improving the range resolution through pulse compression, linearly frequency modulated (LFM) waveforms are widely applied in modern radar systems [1,2]. However, the conventional LFM signal would lead to the range–Doppler coupling effect [3–6] due to the knife-edge-shape ambiguity function. To solve this problem, LFM signals composed of two complementary chirped waveforms [7], or the frequency modulated signals with linear up- and down-chirp rate alternatively [8], were proposed. Generally, an LFM signal composed of two complementary chirped waveforms (i.e., dual-chirp LFM signal) can be generated by using a scanning microwave oscillator or a direct digital synthesizer in the electrical domain [9]. However, the center frequency and the bandwidth of the generated signal are restricted by the limited bandwidth of the microwave devices. Photonic approaches have been widely used to generate LFM signals due to the advantages of high frequency, large bandwidth, and parallel processing introduced by photonics [10,11].

The generation of dual-chirp LFM signal can be realized by introducing a baseband single-chirp LFM signal and a local oscillator (LO) signal to the two sub-Mach–Zehnder modulators (MZMs) of a dual-parallel MZM [12] or a dual-polarization quadrature phase shift keying modulator [13]. Both of the two sub-MZMs are biased at the minimum transmission point. By injecting the output of the integrated modulator into a photodetector (PD), two complementarily chirped microwave waveforms will be generated, with the center frequency upconverted to the frequency of the LO. Two cascaded MZMs biased at the minimum transmission point can also be used to achieve the dual-chirp LFM signal generation [14,15]. However, for these approaches [12–15], a wideband microwave arbitrary waveform generator and a high-frequency microwave source are required. In order to solve this problem, the generation of the frequency modulated signals with linear up- and down-chirp rate alternatively (i.e., triangular frequency modulated microwave waveform) can be implemented using an optoelectronic oscillator (OEO) incorporating a frequency-scanning

electrical bandpass filter [16]. However, the bandwidth of the generated signal is relatively small. In addition, the frequency and the time duration are determined by the oscillation frequency and the loop length of the OEO, respectively, resulting in limited tunability.

Recently, we have proposed a method to generate a triangular frequency modulated microwave waveform based on an optically injected semiconductor laser [17]. By setting the electrical control signal to have a triangular profile, the injected light has an alternate linearly increasing and decreasing optical amplitude. With the semiconductor laser operating at the period-one (P1) oscillation state, a triangular frequency modulated microwave waveform will be generated after the optical-electrical conversion. Only a low-frequency electrical device is needed to provide the low-frequency triangular control waveform. However, in our reported paper, there are only some preliminary experimental results. In order to understand the approach in-depth, in this paper, comprehensive theoretical and experimental investigations are taken. A method based on a generalized regression neural network is also proposed to improve the linearity of the generated waveform. A proof-of-concept experiment is carried out. Triangular frequency modulated microwave waveforms with a frequency range from 14–24 GHz and a time duration of 2 μs have been successfully generated. The improvement of the linearity of the waveform is experimentally verified. The performance of the generated triangular frequency modulated microwave waveforms for reducing the range–Doppler coupling is also verified. In addition, the tunability of the bandwidth, the center frequency, and the time duration is experimentally demonstrated.

2. PRINCIPLE

Figure 1 shows the schematic diagram of the proposed system to generate a triangular frequency modulated microwave waveform. A continuous-wave light generated from a master laser (ML) is sent to an MZM via an optical attenuator (ATT). A low-frequency electrical triangular control signal generated from a direct digital synthesizer is applied to the MZM to modulate the continuous-wave light, which is then injected into the slave laser (SL) through a polarization controller (PC) and a circulator. By properly setting the wavelength of the ML, the attenuation of the ATT, and the state of the PC, the SL will operate at the P1 oscillation state. The light wave emitted from the SL contains several longitudinal modes with fixed wavelength spacing, which is determined by the injection parameter ξ [10], defined as the square root of the power ratio between the injected light and light emitting from the free-running SL. Through applying the electrical triangular control signal to the MZM, the power of the injection light output from the MZM, as well as the injection parameter ξ, will increase and decrease with time, corresponding with the rising and the falling edges of the triangular waveform, respectively. Thus, the wavelength spacing of the light wave emitted from the SL will also increase and decrease with time, correspondingly. By injecting the optical output into a PD, the optical-electrical conversion will be realized, and a triangular frequency modulated microwave waveform will be generated.

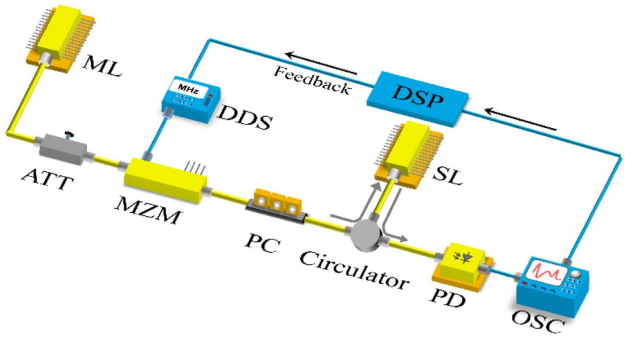

Fig. 1. Schematic of the proposed system to generate a triangular frequency modulated microwave waveform. ML: master laser, Agilent N7714A; ATT: optical attenuator, EXFO FVA-600; MZM: Mach–Zehnder modulator Lucent, 10 Gb/s; DDS: direct digital synthesizer, Agilent 33250A; PC: polarization controller; SL: slaver laser, Actech LD15DM; PD: photodetector, u^2t XPDV2120RA; OSC: oscilloscope, Keysight DSO-X 92504A.

Mathematically, the electrical triangular control signal applied to the MZM is expressed as

$$s_{\mathrm{tri}}(t)=\begin{cases}\frac{2V_{\mathrm{pp}}}{T_{\mathrm{tri}}}t+\frac{V_{\mathrm{pp}}}{2}+V_{\mathrm{offset}}, & -\frac{T_{\mathrm{tri}}}{2}\le t\le 0\\ -\frac{2V_{\mathrm{pp}}}{T_{\mathrm{tri}}}t+\frac{V_{\mathrm{pp}}}{2}+V_{\mathrm{offset}}, & 0\le t\le\frac{T_{\mathrm{tri}}}{2}\end{cases}, \tag{1}$$

where V_{pp}, V_{offset}, and T_{tri} are the peak-to-peak value, the offset value, and the time duration of the control signal, respectively. The optical power transmission function of the MZM [17–19] can be written as

$$T_{\mathrm{MZM}}[V(t)]=\frac{1}{2}\left[1+\cos\left(\Delta\varphi+\pi\frac{V(t)}{V_{\pi}}\right)\right], \tag{2}$$

where $V(t)$ is the microwave signal that is applied to the MZM and $\Delta\varphi$ is the phase introduced by the bias voltage. Thus, the injection parameter can be calculated, expressed as

$$\xi(t)=\sqrt{\frac{P_{\mathrm{inj}}(t)}{P_{\mathrm{SL}}}}=\sqrt{\frac{P_{\mathrm{ML}}L_{\mathrm{ATT}}T_{\mathrm{MZM}}[s_{\mathrm{tri}}(t)]}{P_{\mathrm{SL}}}}, \tag{3}$$

where $P_{\mathrm{inj}}(t)$ is the power of the injected light, P_{ML} and P_{SL} are the powers of the lights emitted from ML and the free-running SL, respectively, and L_{ATT} is the introduced optical amplitude loss of the system. As has been demonstrated in [10,20–23], at the P1 oscillation state, the wavelength spacing of the optical signal emitted from the SL monotonically increases with ξ. For a detailed mathematical deduction, we introduce a function named as H(∗), which represents the relationship between the frequency of the generated microwave signal and the square of the injection parameter. It is obvious that H(∗) is also a monotonically increasing function with ξ^2. At the same time, $\Delta\varphi$ in Eq. (2) can be added into the $V(t)$ in Eq. (1), leading to the equivalent offset value of the control signal, which is expressed as $V'_{\mathrm{offset}}=(V_{\pi}\Delta\varphi)/\pi+V_{\mathrm{offset}}$. Thus, the frequency of the generated signal after the PD can be expressed as

$$f(t)=\mathrm{H}\{\xi^2(t)\}=\mathrm{H}\left\{\frac{P_{\mathrm{ML}}L_{\mathrm{ATT}}T_{\mathrm{MZM}}[s_{\mathrm{tri}}(t)]}{P_{\mathrm{SL}}}\right\}=\begin{cases}\mathrm{H}\left\{\frac{P_{\mathrm{ML}}L_{\mathrm{ATT}}}{2P_{\mathrm{SL}}}\left[1+\cos\left(\pi\frac{V'_{\mathrm{offset}}}{V_\pi}+\pi\frac{2V_{\mathrm{pp}}t}{V_\pi T_{\mathrm{tri}}}+\pi\frac{V_{\mathrm{pp}}}{2V_\pi}\right)\right]\right\}, & -\frac{T_{\mathrm{tri}}}{2}\le t\le 0\\ \mathrm{H}\left\{\frac{P_{\mathrm{ML}}L_{\mathrm{ATT}}}{2P_{\mathrm{SL}}}\left[1+\cos\left(\pi\frac{V'_{\mathrm{offset}}}{V_\pi}-\pi\frac{2V_{\mathrm{pp}}t}{V_\pi T_{\mathrm{tri}}}+\pi\frac{V_{\mathrm{pp}}}{2V_\pi}\right)\right]\right\}, & 0\le t\le\frac{T_{\mathrm{tri}}}{2}\end{cases}. \tag{4}$$

When the modulated triangular control signal is a small signal, i.e., $V_{\mathrm{pp}}\ll V_\pi$, and $V'_{\mathrm{offset}}\neq 0,\pi$, the frequency of the generated microwave signal can be written as

$$\begin{aligned}f(t)&=\begin{cases}\mathrm{H}\left\{\frac{P_{\mathrm{ML}}L_{\mathrm{ATT}}}{2P_{\mathrm{SL}}}\left[1+\cos\left(\pi\frac{V'_{\mathrm{offset}}}{V_\pi}\right)-\sin\left(\pi\frac{V'_{\mathrm{offset}}}{V_\pi}\right)\left(\pi\frac{2V_{\mathrm{pp}}t}{V_\pi T_{\mathrm{tri}}}+\pi\frac{V_{\mathrm{pp}}}{2V_\pi}\right)\right]\right\}\\ \text{when } -\frac{T_{\mathrm{tri}}}{2}\le t\le 0\\ \mathrm{H}\left\{\frac{P_{\mathrm{ML}}L_{\mathrm{ATT}}}{2P_{\mathrm{SL}}}\left[1+\cos\left(\pi\frac{V'_{\mathrm{offset}}}{V_\pi}\right)-\sin\left(\pi\frac{V'_{\mathrm{offset}}}{V_\pi}\right)\left(-\pi\frac{2V_{\mathrm{pp}}t}{V_\pi T_{\mathrm{tri}}}+\pi\frac{V_{\mathrm{pp}}}{2V_\pi}\right)\right]\right\}\\ \text{when } 0\le t\le\frac{T_{\mathrm{tri}}}{2}\end{cases}\\ &=\begin{cases}\mathrm{H}(P_0)+\mathrm{H}'(P_0)\left[-\sin\left(\pi\frac{V'_{\mathrm{offset}}}{V_\pi}\right)\right]\left(\pi\frac{2V_{\mathrm{pp}}t}{V_\pi T_{\mathrm{tri}}}+\pi\frac{V_{\mathrm{pp}}}{2V_\pi}\right), & -\frac{T_{\mathrm{tri}}}{2}\le t\le 0\\ \mathrm{H}(P_0)+\mathrm{H}'(P_0)\left[-\sin\left(\pi\frac{V'_{\mathrm{offset}}}{V_\pi}\right)\right]\left(-\pi\frac{2V_{\mathrm{pp}}t}{V_\pi T_{\mathrm{tri}}}+\pi\frac{V_{\mathrm{pp}}}{2V_\pi}\right), & 0\le t\le\frac{T_{\mathrm{tri}}}{2}\end{cases}\\ &=\begin{cases}f_c+k\left(\pi\frac{2V_{\mathrm{pp}}t}{V_\pi T_{\mathrm{tri}}}+\pi\frac{V_{\mathrm{pp}}}{2V_\pi}\right), & -\frac{T_{\mathrm{tri}}}{2}\le t\le 0\\ f_c+k\left(-\pi\frac{2V_{\mathrm{pp}}t}{V_\pi T_{\mathrm{tri}}}+\pi\frac{V_{\mathrm{pp}}}{2V_\pi}\right), & 0\le t\le\frac{T_{\mathrm{tri}}}{2}\end{cases},\end{aligned} \tag{5}$$

where $P_0=P_{\mathrm{ML}}L_{\mathrm{ATT}}[1+\cos(\pi V'_{\mathrm{offset}}/V_\pi)]/2P_{\mathrm{SL}}$, $f_c=\mathrm{H}(P_0)$, and $k=\mathrm{H}'(P_0)[-\sin(\pi V'_{\mathrm{offset}}/V_\pi)]$, where $\mathrm{H}'(*)$ is the first derivative of $\mathrm{H}(*)$. Thus, a triangular frequency modulated microwave waveform is generated, with a center frequency of f_c, a bandwidth of $k\pi V_{\mathrm{pp}}/V_\pi$, and a time duration of T_{tri}. As a result, on the condition of small signal approximation, by adjusting the values of V_{offset} (or L_{ATT}), V_{pp} and T_{tri}, the center frequency, bandwidth, and time duration of the generated triangular frequency modulated microwave waveform can be adjusted, respectively.

3. EXPERIMENTAL RESULTS AND DISCUSSIONS

Based on the scheme shown in Fig. 1, an experiment is carried out. An optical carrier with a wavelength of 1552.009 nm is generated from an ML (Agilent N7714A) and sent to an MZM (Lucent, 10 Gb/s) with a half-wave voltage of 3.2 V. Using a 120 MHz arbitrary waveform generator (Agilent 33250A), the electrical control signal is generated and applied to the MZM. The bias current and the control temperature of the SL (Actech LD15DM) are 34.1 mA and 12.545°C, respectively. A 40 GHz PD (u^2t XPDV2120RA) is used to realize the optical-electrical conversion. The output of the PD is sent to an 80 GSa/s real-time oscilloscope (Keysight DSO-X 92504A). In the experiment, an optical spectrum analyzer (APEX AP2040D) with a resolution of 0.04 pm is utilized to measure the spectra of the optical signals.

The spectra of the optical signals from the ML and the free-running SL are shown in Fig. 2(a). The wavelengths of the ML and the free-running SL are 1552.009 and 1552.027 nm, respectively. By setting the state of the PC and the optical attenuator to make the SL operate at the P1 state, the spectrum of the light from the injected SL is shown in Fig. 2(b). As can be seen, the light wave emitted from the SL contains several longitudinal modes with a fixed wavelength spacing, which is determined by the power of the injection light. When the power of the injected light is 2.01 dBm, the mode spacing of the output of the SL is 0.139 nm (corresponding to 17.33 GHz), as shown in Fig. 2(b). After injecting the light from the SL into a PD, a microwave waveform with a frequency of 17.33 GHz will be generated.

To generate the triangular frequency modulated microwave waveform, an electrical triangular control signal with V_{pp} of 2.5 V and V_{offset} of −0.55 V, shown in Fig. 3(a), is applied to the MZM. The temporal waveform and the instantaneous frequency-time diagram of the generated triangular frequency modulated microwave waveform are shown in Figs. 3(b) and 3(c), respectively. As can be seen, the generated triangular frequency modulated microwave waveform is composed of two

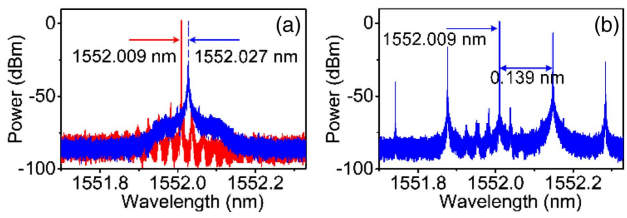

Fig. 2. (a) Spectra of optical signals from the ML (red curve) and the free-running SL (blue dashed curve). (b) Spectrum of the optical signal from the injected SL.

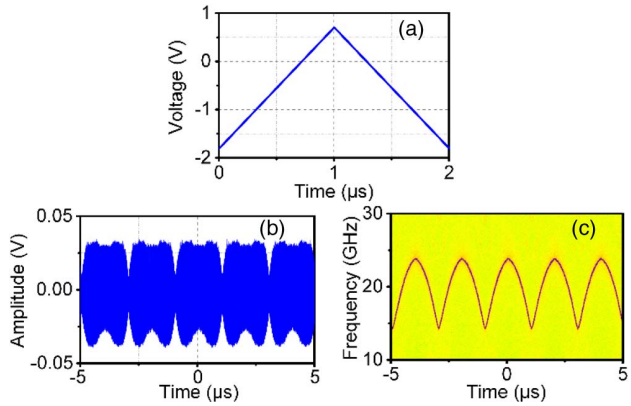

Fig. 3. (a) Waveform of the electrical triangular control signal. (b) The generated temporal waveform and (c) the corresponding instantaneous frequency-time diagram of the obtained triangular frequency modulated microwave waveform.

complementary chirped waveforms, the instantaneous frequencies of which increase from 14 to 24 GHz and decrease from 24–14 GHz, respectively. The time duration is 2 μs, equal to the time period of the applied electrical triangular control signal.

One key problem of the proposed approach is that the linearity of the generated triangular frequency modulated microwave waveform is very poor, as can be seen in Fig. 3(c), for the fact that the small signal modulation assumption to achieve Eq. (5) is not satisfied. Mathematically, the linearity of a signal is the ratio between the maximal frequency deviation from the idealized frequency and the bandwidth of the signal [24], presenting the degree of the frequency offset from the ideal linear frequency. Thus, the linearity of the generated signal can be calculated to be 0.132. In order to improve the linearity of the generated waveform, a method based on a generalized regression neural network is proposed. The flow diagram of the modification is shown in Fig. 4. First, a generalized regression neural network is used as the response function of the simulation system, to fit the measured transmission function between the frequency of the generated waveform and the offset voltage of the electrical control signal. An ideal triangular control signal is used as the input signal to the simulation system. The corresponding instantaneous frequency of the output is obtained. Then, the error between the instantaneous frequency of the output signal and the ideal triangular frequency modulated microwave waveform is calculated. When the error is larger than the minimum tolerance (*eps*), a correction of the voltage is applied to reduce the error. If overcorrection occurs, a smaller correction step size is set and an opposing correction is carried out. Once the error is smaller than *eps*, the modification process is interrupted. A modified control signal is therefore obtained to generate the triangular frequency modulated microwave waveform with improved linearity.

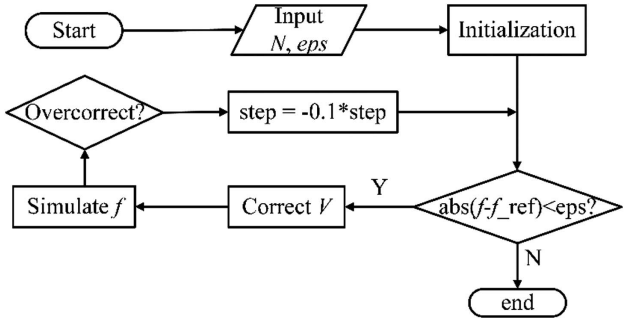

Fig. 4. Flow diagram of the negative feedback. N, sampling point number; eps, minimum tolerance; V, the voltage of the initial control signal; f_ref, the ideal instantaneous frequency; step, the correction step size; f, the instantaneous frequency of the generated signal.

First, the relationship between the frequency of the generated microwave waveform and the injected optical power is experimentally obtained. The variety of injected optical power is realized by changing the voltage of the electrical control signal. By setting V_{pp} of the electrical signal $S_{tri}(t)$ in Eq. (1) to be 0, V_{offset} is actually the voltage of the control signal. The measured results between the frequency of the generated signal and the voltage of the control signal are shown in Fig. 5. It can be seen that as the voltage of the control signal increases from −1.8 to 0.7 V, the frequency of the generated signal increases from 13.34 to 24.01 GHz. Then the frequency of the generated signal decreases from 24.01 to 13.34 GHz with the voltage of the control signal increasing from 0.7 to 3.2 V. The voltage range for which the frequency of the generated signal monotonically increases or decreases is determined by the transmission function of the MZM.

Based on the modification process shown in Fig. 4, a generalized regression neural network is used as the response function of the simulation system, to fit the measured transmission function between the frequency of the generated signal and the offset voltage of the electrical control signal, as shown in Fig. 5. Then an ideal triangular control signal is generated as the input signal to the simulation system, as illustrated in Fig. 6(a). The corresponding instantaneous frequency of the output is shown as the blue solid line in Fig. 6(b). The red dashed line in Fig. 6(b) is the ideal instantaneous frequency of a triangular frequency modulated microwave waveform. Based on the modification process shown in Fig. 4, the modified control signal is obtained as shown in Fig. 6(c) and the instantaneous frequency of the generated signal is shown in Fig. 6(d).

After the modification process, the experimental modified electrical triangular control signal shown in Fig. 7(a) is applied to the MZM. The corresponding waveform and the instantaneous

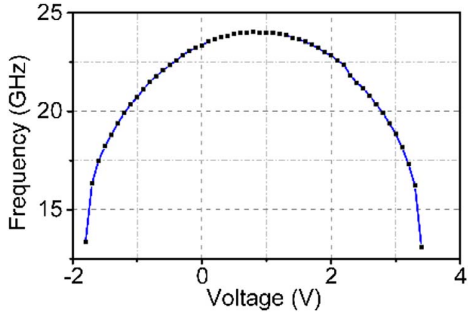

Fig. 5. Relationship between the frequency of the generated microwave waveform and the offset voltage of the electrical control signal.

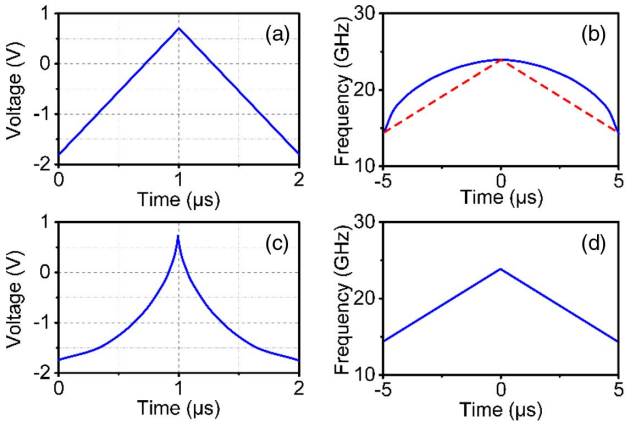

Fig. 6. (a) Ideal triangular control signal; (b) the simulated instantaneous frequency of the generated waveform (blue solid line) and the ideal one (red dashed line); (c) the modified triangular control signal; and (d) the simulated instantaneous frequency of the generated waveform after modification.

frequency-time diagram of the generated triangular frequency modulated microwave waveform signal with a time duration of 2 μs are shown in Figs. 7(b) and 7(c), respectively. The linearity of the results shown in Fig. 7(c) is calculated to be 0.025. Compared with the result shown in Fig. 3(c), the linearity of the generated triangular frequency modulated microwave waveform has been significantly improved.

To demonstrate the performance of the triangular frequency modulated microwave waveform for reducing the range–Doppler coupling, the ambiguity function of the generated triangular frequency modulated microwave waveform and the corresponding contour map are illustrated in Figs. 8(a1)–8(c1). As a comparison, the ambiguity function of an ideal single-chirp LFM signal and the corresponding contour map with the same frequency span and time duration are also calculated, with the results shown in Figs. 8(a2)–8(c2). From Fig. 8 we can see that the ambiguity function of the single-chirp LFM signal has a knife-edge shape, while that of the generated triangular

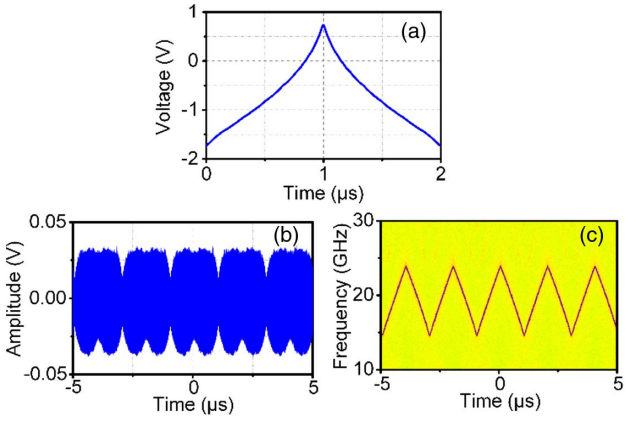

Fig. 7. (a) Temporal waveform of the modified electrical control signal. (b) The temporal waveform, and (c) the corresponding instantaneous frequency-time diagram of the obtained triangular frequency modulated microwave waveform.

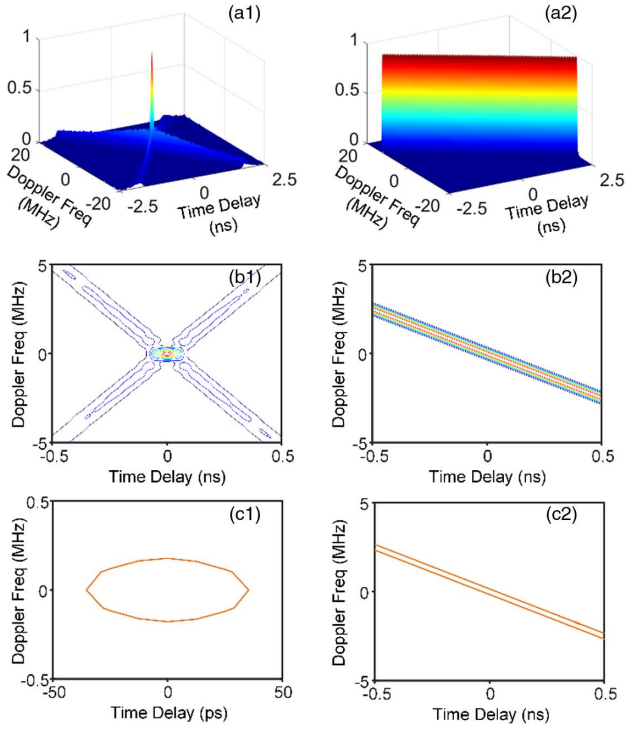

Fig. 8. (a) Ambiguity function, (b) the corresponding contour map, and (c) the −3-dB contour map of (1) the generated triangular frequency modulated microwave waveform after the modification process, and (2) an ideal single-chirp LFM signal with the same frequency range of 14–24 GHz and the same time duration of 2 μs.

frequency modulated microwave waveform signal has a thumbtack shape, reducing the range–Doppler coupling effect.

The tunability of the time duration, bandwidth, and center frequency of the generated triangular frequency modulated microwave waveform is also verified, with the results shown in Fig. 9. First, the tunability of the time duration is realized by tuning the time duration of the control signal. By setting the offset voltage V_{offset} to be −1.65 V and V_{pp} value to be 0.2 V, the triangular frequency modulated microwave waveform with a bandwidth of 2.7 GHz centered at 16.3 GHz will be generated, as shown in Figs. 9(a)–9(d). The time duration of the generated signal is tuned from 0.5 to 4 μs when the time duration of the electrical triangular control signal is tuned.

Then the tuning of the bandwidth is performed through changing the peak-to-peak voltage V_{pp} of the control signal, which is set to be 0.1, 0.2, 0.3, and 0.4 V, respectively. The time duration and the offset voltage are kept to be 2 μs and −1.6 V. The corresponding instantaneous frequency-time diagrams of the generated signals are shown in Figs. 9(e)–9(h). As can be seen, the corresponding bandwidths are tuned to be 0.5, 0.9, 2, and 4.6 GHz, respectively, and the time duration and the center frequency of the generated triangular frequency modulated microwave waveform signals are kept to be 2 μs and 16.2 GHz.

In addition, the tunability of the center frequency is verified by adjusting the injected optical power. The time duration, the offset voltage V_{offset}, and the peak-to-peak voltage V_{pp} of the electrical triangular signal are kept to be 2 μs, −1.75 V, and

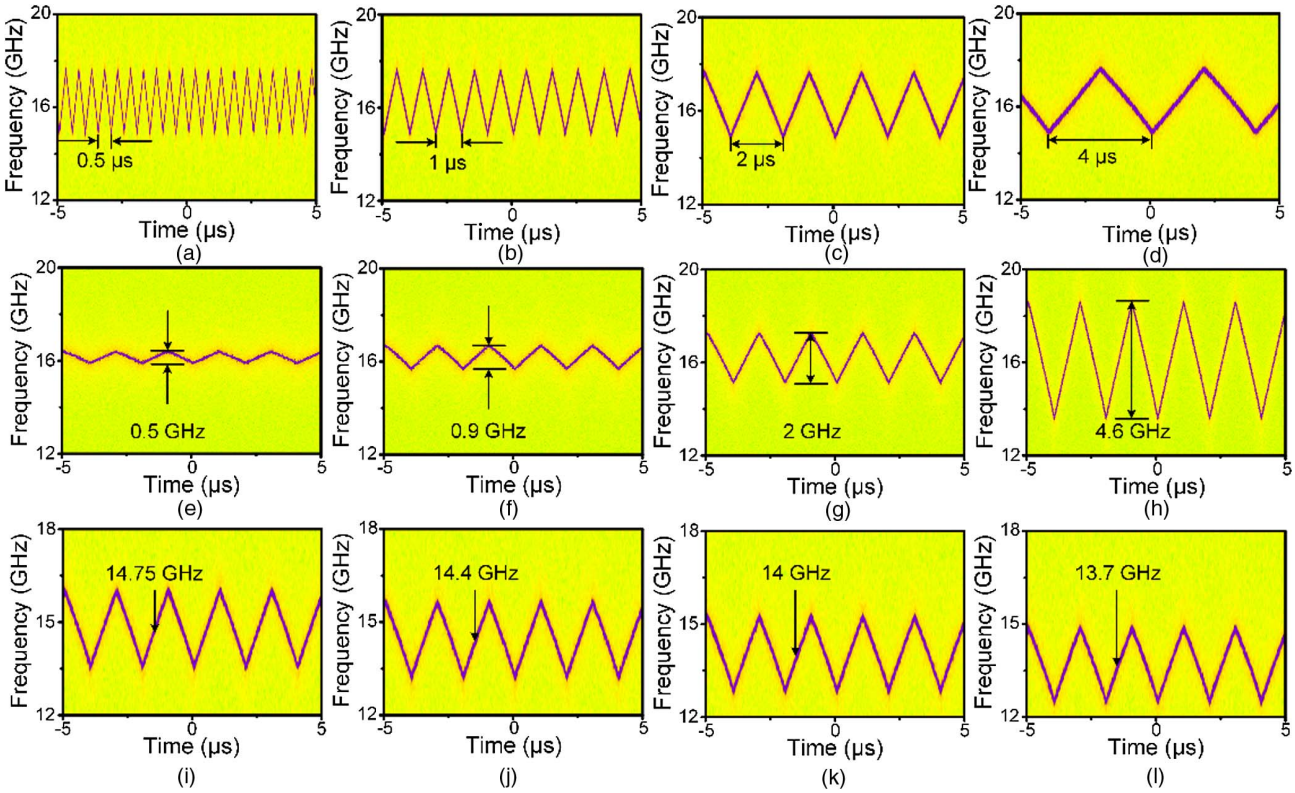

Fig. 9. Instantaneous frequency-time diagrams of the generated triangular frequency modulated microwave waveforms with (a)–(d) the time duration tuning from 0.5 to 4 μs, (e)–(h) the bandwidth tuning from 0.5 to 4.6 GHz, and (i)–(l) the center frequency tuning from 13.7 to 14.75 GHz.

0.1 V. By setting the attenuation of the optical attenuator to be 0, 0.5, 1, and 1.5 dB, respectively, the generated triangular frequency modulated microwave waveforms are shown in Figs. 9(i)–9(l) correspondingly. The center frequencies of the triangular frequency modulated microwave waveforms are 14.75, 14.4, 14, and 13.7 GHz, respectively, and the time duration and the bandwidth are kept to be 2 μs and 2.5 GHz. Except for the frequency tuning range and bandwidth, the frequency stability and the phase noise of the generated microwave signals are also critical parameters to apply this technology into the actual systems. Methods of optoelectronic feedback can be applied to further improve the phase noise and the frequency stability performances of the generated microwave signals [25–27].

It is also worthy to note that in our experiments, the frequency range of the generated triangular frequency modulated microwave waveform signal is only from 13.34–24.01 GHz, which is limited by the characteristics of the used SL. Based on the research in [28], through using a semiconductor laser with a larger linewidth enhancement factor, the frequency range of the generated triangular frequency modulated microwave waveform can be further extended.

4. CONCLUSION

In conclusion, a photonics-based triangular frequency modulated microwave waveform generator is proposed and experimentally demonstrated. The key contribution of the approach is that only a low-frequency electrical triangular control waveform is needed to generate a triangular frequency modulated microwave waveform with large bandwidth, high frequency, large time duration, and good tunability. A triangular frequency modulated microwave waveform with a frequency span from 14–24 GHz and a time duration of 2 μs has been successfully generated. The tunability of the bandwidth, center frequency, and time duration is also experimentally demonstrated. A modification process is carried out to improve the linearity of the signal. The improvement with the range–Doppler resolution by using the generated triangular frequency modulated microwave waveform is verified. The proposed approach can find applications in radar systems. In addition, the photonic approach to generate the triangular frequency modulated microwave waveform can be combined with the radio over fiber techniques and find applications in photonic-assisted distributed radar systems.

Funding. Natural Science Foundation of Jiangsu Province (BK20160082); Jiangsu Provincial Program for High-level Talents in Six Areas (DZXX-030); Jiangsu Provincial "333" Project (BRA2018042); Fundamental Research Funds for Central Universities (NC2018005, NE2017002).

REFERENCES

1. M. A. Richards, *Fundamentals of Radar Signal Processing* (McGraw-Hill, 2014).

2. F. Z. Zhang, Q. S. Guo, Z. Q. Wang, P. Zhou, G. Q. Zhang, J. Sun, and S. L. Pan, "Photonics-based broadband radar for high-resolution and real-time inverse synthetic aperture imaging," Opt. Express **25**, 16274–16281 (2017).
3. M. I. Skolnik, *Introduction to Radar Systems* (McGraw-Hill, 2001).
4. R. J. Fitzgerald, "Effects of range-Doppler coupling on chirp radar tracking accuracy," IEEE Trans. Aerosp. Electron. Syst. **AES-10**, 528–532 (1974).
5. L. Bruno, P. Braca, J. Horstmann, and M. Vespe, "Experimental evaluation of the range-Doppler coupling on HF surface wave radars," IEEE Geosci. Remote Sens. Lett. **10**, 850–854 (2013).
6. G. Li, H. D. Meng, X. G. Xia, and Y. N. Peng, "Range and velocity estimation of moving targets using multiple stepped-frequency pulse trains," Sensors **8**, 1343–1350 (2008).
7. A. Amar and Y. Buchris, "Asynchronous transmitter position and velocity estimation using a dual linear chirp," IEEE Signal Process. Lett. **21**, 1078–1082 (2014).
8. S. Kim, I. Paek, and M. Ka, "Simulation and test results of triangular fast ramp FMCW waveform," in *Proceedings of IEEE Radar Conference (RADAR)* (2003), pp. 1–4.
9. H. Kwon and B. Kang, "Linear frequency modulation of voltage-controlled oscillator using delay-line feedback," IEEE Microwave Wireless. Compon. Lett. **15**, 431–433 (2005).
10. P. Zhou, F. Z. Zhang, Q. S. Guo, and S. L. Pan, "Linearly chirped microwave waveform generation with large time-bandwidth product by optically injected semiconductor laser," Opt. Express **24**, 18460–18467 (2016).
11. W. J. Chen, D. Zhu, C. X. Xie, T. Zhou, X. Zhong, and S. L. Pan, "Photonics-based reconfigurable multi-band linearly frequency-modulated signal generation," Opt. Express **26**, 32491–32499 (2018).
12. D. Zhu and J. P. Yao, "Dual-chirp microwave waveform generation using a dual-parallel Mach-Zehnder modulator," IEEE Photonics Technol. Lett. **27**, 1410–1413 (2015).
13. X. Li, S. H. Zhao, Z. H. Zhu, K. Qu, T. Lin, and D. P. Hu, "Photonic generation of frequency and bandwidth multiplying dual-chirp microwave waveform," IEEE Photonics J. **9**, 1–14 (2017).
14. R. Kumar and S. K. Raghuwanshi, "A photonic scheme for the generation of dual linear chirp microwave waveform based on the external modulation technique and its airborne application," Opt. Quantum Electron. **49**, 370 (2017).
15. Y. X. Xu, T. Jin, H. Chi, S. L. Zheng, X. F. Jin, and X. M. Zhang, "Photonic generation of dual-chirp waveforms with improved time-bandwidth product," IEEE Photonics Technol. Lett. **29**, 1253–1256 (2017).
16. Q. Z. Cen, Y. T. Dai, F. F. Yin, Y. Zhou, J. Q. Li, J. Dai, L. Yu, and K. Xu, "Rapidly and continuously frequency-scanning opto-electronic oscillator," Opt. Express **25**, 635–643 (2017).
17. B. W. Zhang, D. Zhu, and S. L. Pan, "Dual-chirp microwave waveform generation for radar application based on an optically injected semiconductor laser," in *Proceedings of the 5th IEEE MTT-S International Wireless Symposium (IWS)* (2018).
18. P. Dong, S. R. Liao, D. Z. Feng, H. Liang, D. W. Zheng, R. Shafiiha, C. C. Kung, W. Qian, G. L. Li, X. Z. Zheng, A. V. Krishnamoorthy, and M. Asghari, "Low V_{pp}, ultralow-energy, compact, high-speed silicon electro-optic modulator," Opt. Express **17**, 22484–22490 (2009).
19. K. K. Xu, "Silicon MOS optoelectronic micro-nano structure based on reverse-biased PN junction," Phys. Status Solidi A **216**, 1800868 (2019).
20. S. K. Hwang, J. M. Liu, and J. K. White, "Characteristics of period-one oscillations in semiconductor lasers subject to optical injection," IEEE J. Sel. Top. Quantum Electron. **10**, 974–981 (2004).
21. S. C. Chan, "Analysis of an optically injected semiconductor laser for microwave generation," IEEE J. Quantum Electron. **46**, 421–428 (2010).
22. P. P. Yupapin and S. Suchat, "Entangle photon generation using fiber optic Mach-Zehnder interferometer incorporating nonlinear effect in a fiber ring resonator," J. Nanophotonics **1**, 013504 (2007).
23. K. K. Xu, L. Huang, Z. Y. Zhang, J. M. Zhao, Z. P. Zhang, L. W. Snyman, and J. W. Swart, "Light emission from a poly-silicon device with carrier injection engineering," Mater. Sci. Eng. B **231**, 28–31 (2018).
24. J. W. Song, "A technique for measuring the linearity of a linearly frequency-modulated signal," J. Electron. **12**, 66–72 (1995).
25. S. C. Chan and J. M. Liu, "Tunable narrow-linewidth photonic microwave generation using semiconductor laser dynamics," IEEE J. Sel. Top. Quantum Electron. **10**, 1025–1032 (2004).
26. J. P. Zhuang and S. C. Chan, "Tunable photonic microwave generation using optically injected semiconductor laser dynamics with optical feedback stabilization," Opt. Lett. **38**, 344–346 (2013).
27. J. Suelzer, T. B. Simpson, P. S. Devgan, and N. G. Usechak, "Tunable, low-phase-noise microwave signals from an optically injected semiconductor laser with opto-electronic feedback," Opt. Lett. **42**, 3181–3184 (2017).
28. S. K. Hwang and D. H. Liang, "Effects of linewidth enhancement factor on period-one oscillations of optically injected semiconductor lasers," Appl. Phys. Lett. **89**, 061120 (2006).